# On Finding Spherical Geodesic Paths and Circles in $\mathbb{Z}^3$

Ranita Biswas and Partha Bhowmick

Department of Computer Science and Engineering
Indian Institute of Technology, Kharagpur, India
{biswas.ranita,bhowmick}@gmail.com

**Abstract.** A *discrete spherical geodesic path* between two voxels $s$ and $t$ lying on a discrete sphere is a/the 1-connected shortest path from $s$ to $t$, comprising voxels of the discrete sphere intersected by the real plane passing through $s$, $t$, and the center of the sphere. We show that the set of sphere voxels intersected by the aforesaid real plane always contains a *1-connected cycle* passing through $s$ and $t$, and each voxel in this set lies within an isothetic distance of $\frac{3}{2}$ from the concerned plane. Hence, to compute the path, the algorithm starts from $s$, and iteratively computes each voxel $p$ of the path from the predecessor of $p$. A novel number-theoretic property and the 48-symmetry of discrete sphere are used for searching the *1-connected* voxels comprising the path. The algorithm is *output-sensitive*, having its time and space complexities both linear in the length of the path. It can be extended for constructing 1-connected discrete 3D circles of arbitrary orientations, specified by a few appropriate input parameters. Experimental results and related analysis demonstrate its efficiency and versatility.

**Keywords:** Discrete sphere, geodesic path, geometry of numbers, discrete 3D circles.

## 1 Introduction

The shortest path between two points on a curved surface is called *geodesic*. There exist several works related to geodesics on a 3D triangulated surface, e.g., the fast marching technique [8]. This technique and *Polthier's straightest geodesics theory* [13] are used in [11] for finding *approximate geodesics* on triangulated surfaces. For exact geodesics, a cubic-time *line-of-sight algorithm* is proposed in [1].

The first algorithm to solve the discrete geodesic problem as the shortest path (SP) between a source and a destination point on an arbitrarily polyhedral surface is referred in the literature as MMP [12]. The discrete surface points are first preprocessed and stored in a suitable data structure in $O(n^2 \log n)$ time, and then the actual SP is reported by *continuous Dijkstra's algorithm* in $O(k + \log n)$ time, where $n = \#$edges on the surface and $k = \#$faces crossed by SP. Improving MMP to $O(n^2)$ time complexity is done in CH algorithm [4] using a set of

E. Barcucci et al. (Eds.): DGCI 2014, LNCS 8668, pp. 396–409, 2014.

windows on the polyhedron edges for encoding the shortest paths. However, it is shown in [14] that MMP, in practice, runs faster than CH. Later, it has been shown in [16] that CH can be made to run faster than MMP, using priority queue and filtering out the useless windows. Recently, a parallel version of CH is proposed in [19]. Further developments with graph-theoretic and numerical methodologies may be seen in [17, 18].

Problems related to geodesic paths and their characterization in the digital space have gained significant attention in recent time. In [5], a new geodesic metric and the $A^*$ *algorithm* are used to find the shortest path between a source and a destination voxel. In [3], *rubberband algorithm* is proposed for computation of minimum-length polygonal curves in cube-curves in 3D space. The idea can be extended to solve various Euclidean shortest path (ESP) problems inside of a simple cube arc, inside of a simple polygon, on the surface of a convex polytope, or inside of a simply-connected polyhedron [10].

In $\mathbb{R}^3$, a *spherical geodesic path* is defined between two points $p \in \mathbb{R}^3$ and $q \in \mathbb{R}^3$ lying on a real sphere $S_r^{\mathbb{R}}$ of radius $r$. The path always lies along the intersection circle of $S_r^{\mathbb{R}}$ and the 3D plane passing through $p$, $q$, and the center of $S_r^{\mathbb{R}}$. We make an analogous definition for *discrete spherical geodesic path* $\boldsymbol{\pi}_r^{\mathbb{Z}}(s,t)$ from a point (voxel) $s \in \mathbb{Z}^3$ to another point $t \in \mathbb{Z}^3$ lying on the discrete sphere, $S_r^{\mathbb{Z}}$, of radius $r$. W.l.o.g., we fix the center of $S_r^{\mathbb{Z}}$ at $o(0,0,0)$, and consider $r$ as a positive integer. Then, $\boldsymbol{\pi}_r^{\mathbb{Z}}(s,t)$ is defined as a/the 1-connected shortest path from $s$ to $t$, comprising only those voxels of $S_r^{\mathbb{Z}}$ which lie sufficiently close to the real plane $\Pi_r^{\mathbb{R}}(s,t)$ passing through $s$, $t$, and $o$.

We first show that there always exists a 1-connected cycle in the set $I_r^{\mathbb{Z}}(s,t)$ comprising the voxels of $S_r^{\mathbb{Z}}$ intersected by $\Pi_r^{\mathbb{R}}(s,t)$. The set $I_r^{\mathbb{Z}}(s,t)$ admits the characterization that all its voxels lie within an isothetic distance of $\frac{3}{2}$ from $\Pi_r^{\mathbb{R}}(s,t)$. Subsequently, $\boldsymbol{\pi}_r^{\mathbb{Z}}(s,t)$ becomes a subset of $I_r^{\mathbb{Z}}(s,t)$, and is efficiently obtained by a prioritized Breadth-First-Search algorithm on the underlying graph corresponding to $I_r^{\mathbb{Z}}(s,t)$. For computation of $I_r^{\mathbb{Z}}(s,t)$, $S_r^{\mathbb{Z}}$ is defined as the irreducible 2-separable set of voxels (3D integer points) that are uniquely identified by certain number-theoretic properties. The algorithm computes the set $I_r^{\mathbb{Z}}(s,t)$ using these properties, without considering the entire set $S_r^{\mathbb{Z}}$. Figure 1 shows a result of our algorithm, where the search space of BFS, its 18 neighborhood on $S_r^{\mathbb{Z}}$, and the final geodesic path $\boldsymbol{\pi}_r^{\mathbb{Z}}(s,t)$ are shown in different colors.

The rest of the paper is organized as follows. Section 2 explains certain elementary number-theoretic properties of a digital sphere, used for computing $I_r^{\mathbb{Z}}(s,t)$. Section 3 contains characterization of discrete spherical geodesic path and circle. The algorithm to compute the geodesic path from a point $s$ to a point $t$ lying on $S_r^{\mathbb{Z}}$ is presented in Section 4. Section 5 contains some test results, and Section 6 the concluding notes.

## 2 Digital Sphere

We first introduce definitions and properties of digital sphere related to this work. These are subsequently used to design the algorithms for finding geodesic

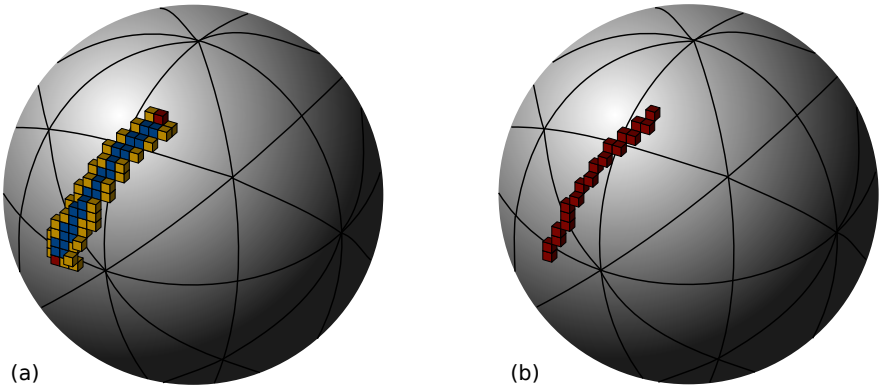


**Fig. 1.** A geodesic path reported by the proposed algorithm for $r = 17$. (a) Red: $s(-6,-1,16)$ and $t(2,14,10)$; blue: $I_r^{\mathbb{Z}}(s,t)$; yellow: 18-neighborhood of the breadth-first search space. (b) The geodesic path $\boldsymbol{\pi}_r^{\mathbb{Z}}(s,t)$ shown in red.

paths and 3D circles in $\mathbb{Z}^3$. The first point to observe is that, opposed to a real sphere, a digital sphere has only nine planes of symmetry. Three of these are the planes containing the *great circles* parallel to three coordinate planes; and for each of these three planes, there exist two more planes aligned at $+45^0$ and $-45^0$ to it. These nine planes of symmetry give rise to eight coordinate octants, called *c-octants*. Each c-octant contains 6 Möbius triangles [7], thus dividing the sphere into 48 *quadraginta octants* or *q-octants*.

### 2.1 Representation

The c-octants and the q-octants are uniquely represented by 3-tuples (see Appendix), which are carefully prepared for efficient implementation of our algorithm. Each c-octant $\mathbb{C}_i$ is represented by a 3-tuple of signs of coordinate axes, namely $C_i := \left(c_i^{(1)}, c_i^{(2)}, c_i^{(3)}\right)$. For example, $C_1 = (+,+,+)$, $C_2 = (-,+,+)$, and so forth. The 3-tuple for each q-octant, on the contrary, represents the three signed coordinate axes. In particular, in the 3-tuple $Q_i := \left(q_i^{(1)}, q_i^{(2)}, q_i^{(3)}\right)$ representing $\mathbb{Q}_i$, each element $q_i^{(\cdot)}$ has two variables, namely $\omega$ and $\sigma$. The variable $\omega$ contains a literal (name of the coordinate axis) from $\{\mathtt{x}, \mathtt{y}, \mathtt{z}\}$, and the variable $\sigma$ contains the sign of the corresponding coordinate. With this representation, we have $Q_1 = (+\mathtt{x}, +\mathtt{y}, +\mathtt{z})$, $Q_2 = (+\mathtt{y}, +\mathtt{x}, +\mathtt{z})$, $Q_3 = (+\mathtt{y}, +\mathtt{z}, +\mathtt{x})$, $\ldots, Q_{24} = (-\mathtt{x}, +\mathtt{z}, -\mathtt{y})$, $\ldots, Q_{48} = (-\mathtt{x}, -\mathtt{z}, -\mathtt{y})$. That is, for $Q_{24}$ as an instance, we have $\omega[q_{48}^{(1)}] = \mathtt{x}$, $\sigma[q_{48}^{(1)}] =$ '$-$', $\omega[q_{48}^{(2)}] = \mathtt{z}$, etc. Our representation ensures the following.

1. $\mathbb{C}_a = \{\mathbb{Q}_b : b = 6(a-1) + c, c = 1, 2, \ldots, 6\}$.
2. Two q-octants $\mathbb{Q}_i$ and $\mathbb{Q}_j$ lie in the same c-octant if and only if $\lceil i/6 \rceil = \lceil j/6 \rceil$ (with $\mathbb{C}_{\lceil i/6 \rceil}$ as their common c-octant).
   Equivalently, $\mathbb{Q}_i$ and $\mathbb{Q}_j$ lie in the same c-octant if and only if $\sigma[q_i] = \sigma[q_j]$ $\forall (q_i, q_j) \in \{(q_i', q_j') : \left((q_i', q_j') \in Q_i \times Q_j\right) \wedge \left(\omega[q_i'] = \omega[q_j']\right)\}$.

3. Let $w = 0$ be one of the three coordinate planes, with $w \in \{x, y, z\}$. Then two c-octants $\mathbb{C}_i$ and $\mathbb{C}_j$ lie in two different half-spaces defined by $w = 0$ if and only if the elements in $C_i$ and $C_j$ corresponding to $w$ are different.

*Example 1.* $C_1(+,+,+)$ and $C_2(-,+,+)$ have their 1st element different, which implies they are in two different half-spaces defined by the coordinate plane $x = 0$; however, their 2nd and 3rd elements being both '+', either of them lies in the half-space $y \geqslant 0$ and in the half-space $z \geqslant 0$.

### 2.2 Metrics

We define *x-distance* and *y-distance* between two (real or integer) points, $p(i, j)$ and $p'(i', j')$, as $d_x(p, p') = |i - i'|$ and $d_y(p, p') = |j - j'|$, respectively. In $\mathbb{R}^3$ or in $\mathbb{Z}^3$, we have also *z-distance*, given by $d_z(p, p') = |k - k'|$, for $p(i, j, k)$ and $p'(i', j', k')$. Using these inter-point distances, we define the respective $x$-, $y$-, and $z$-distances between a point $p(i, j, k)$ and a surface $S$ as follows. Let $d_x(p, S)$ be the $x$-distance between a point $p(i, j, k)$ and a surface $S$. If there exists a point $p'(x', y', z')$ in $S$ such that $(y', z') = (j, k)$, then $d_x(p, S) = d_x(p, p')$; otherwise, $d_x(p, S) = \infty$. The other two distances, i.e., $d_y(p, S)$ and $d_z(p, S)$, are defined in a similar way; note that the metric $d_z(p, S)$ is not defined in 2D. These metrics are used to define the *isothetic distance* as follows.

**Definition 1.** *Between two points $p_1(i_1, j_1)$ and $p_2(i_2, j_2)$, the isothetic distance is taken as the Minkowski norm [9], $d_\infty(p_1, p_2) = \max\{d_x(p_1, p_2), d_y(p_1, p_2)\}$; between a point $p(i, j)$ and a curve $C$, it is $d_\perp(p, C) = \min\{d_x(p, C), d_y(p, C)\}$, where $d_x(p, C)$ and $d_y(p, C)$ are defined similar to $d_x(p, S)$ and $d_y(p, S)$ respectively; between a 3D point $p(i, j, k)$ and a surface $S$, it is $d_\perp(p, S) = \min\{d_x(p, S), d_y(p, S), d_z(p, S)\}$.*

### 2.3 Topology

A *voxel* is an integer point in 3D space, and equivalently, a 3-cell [9]. Two voxels are said to be *0-adjacent* if they share a vertex (0-cell), *1-adjacent* if they share an edge (1-cell), and *2-adjacent* if they share a face (2-cell). Thus, two distinct voxels, $p_1(i_1, j_1, k_1)$ and $p_2(i_2, j_2, k_2)$ are *1-adjacent* if and only if $|i_1 - i_2| + |j_1 - j_2| + |k_1 - k_2| \leqslant 2$ and $\max\{|i_1 - i_2|, |j_1 - j_2|, |k_1 - k_2|\} = 1$; *2-adjacent* if and only if $|i_1 - i_2| + |j_1 - j_2| + |k_1 - k_2| = 1$; and *0-adjacent* if and only if $|i_1 - i_2| = |j_1 - j_2| = |k_1 - k_2| = 1$. Clearly, 0-adjacent (1-adjacent) voxels are not considered as adjacent while considering 1-neighborhood (2-neighborhood) connectivity. Note that the 0-, 1-, and 2-neighborhood notations, as adopted in this paper and also in [15], correspond respectively to the classical 26-, 18-, and 6-neighborhood notations used in [6].

Based on above definitions, a digital sphere is said to be *2-separating* if it does not contain any *2-tunnel*, that is, its interior and exterior are not connected by a *2-connected path* [6]. A 2-separating digital sphere is *irreducible* if and only if it does not contain any *simple voxel*, that is, removal of any voxel violates its

topological property of 2-separableness [6]. We use $S_r^{\mathbb{R}}$ to denote the real sphere of radius $r$ and centered at $o$, use $S_r^{\mathbb{Z}_1}$ to denote the part of $S_r^{\mathbb{Z}}$ lying in $\mathbb{Q}_1$, and use $p \in S_r^{\mathbb{Z}}$ when a voxel $p$ belongs to (voxel set) $S_r^{\mathbb{Z}}$. Our work is based on the following definition of digital sphere.

**Definition 2.** *A digital sphere $S_r^{\mathbb{Z}}$ is an irreducible 2-separating subset of the voxel set having isothetic distance less than $\frac{1}{2}$ from $S_r^{\mathbb{R}}$.*

Note that in [15], the only strict k-separating or irreducible digital sphere results from outer Gaussian digitization, but its voxels are not limited by a maximum isothetic distance of $\frac{1}{2}$ from $S_r^{\mathbb{R}}$. The closed centered 2-separating digitized sphere is another proposition in [15], which is not necessarily irreducible.

### 2.4 Characterization

The characterization of $S_r^{\mathbb{Z}}$ is required to decide in constant time whether a particular voxel $(i, j, k)$ belongs to $S_r^{\mathbb{Z}}$. We start with the following lemmas.

**Lemma 1.** $d_\perp\left(p, S_r^{\mathbb{R}}\right) = \left|k - \sqrt{r^2 - (i^2 + j^2)}\right| \ \forall\ p(i, j, k) \in S_r^{\mathbb{Z}_1}$.

*Proof.* Let $p(i, j, k) \in S_r^{\mathbb{Z}_1}$, and $(x, j, k), (i, y, k)$, and $(i, j, z)$ be the respective points on $S_r^{\mathbb{R}}$ taken along the lines parallel to $x$-, $y$-, and $z$-axes, and passing through $p$. Observe that the points $(x, j, k)$ and $(i, y, k)$ may be nonexistent, but the point $(i, j, z)$ always exists. If all three exist, then

$$x^2 + j^2 + k^2 = i^2 + y^2 + k^2 = i^2 + j^2 + z^2 = r^2, \text{or, } k^2 - z^2 = j^2 - y^2 = i^2 - x^2$$
$$\text{or, } (k + z)(k - z) = (j + y)(j - y) = (i + x)(i - x). \tag{1}$$

In $\mathbb{Q}_1$, $i \leqslant j \leqslant k$ and $x \leqslant y \leqslant z$, or, $i + x \leqslant j + y \leqslant k + z$; so, from Eq. 1,

$$|k - z| \leqslant |j - y| \leqslant |i - x|. \tag{2}$$

If one or both $(x, j, k)$ and $(i, y, k)$ do not exist, then also $|k - z|$ remains the minimum. Hence, from Eq. 2, $d_\perp\left(p, S_r^{\mathbb{R}}\right) = |k - z| = \left|k - \sqrt{r^2 - (i^2 + j^2)}\right|$. □

**Lemma 2.** $d_\perp(p, S_r^{\mathbb{R}}) < \frac{1}{2}\ \forall\ p \in S_r^{\mathbb{Z}}$.

*Proof.* If possible, let, w.l.o.g., $p(i, j, k) \in S_r^{\mathbb{Z}_1}$, such that $\left|k - \sqrt{r^2 - (i^2 + j^2)}\right| = \frac{1}{2}$, or, w.l.o.g., $k - \sqrt{r^2 - (i^2 + j^2)} = -\frac{1}{2}$, which implies $S_r^{\mathbb{R}}$ has $p'(i, j, k + \frac{1}{2})$ as the point of intersection in $\mathbb{Q}_1$ with the 3D straight line $(x = i, y = j)$. Since $(i, j, k + \frac{1}{2})$ lies on $S_r^{\mathbb{R}}$, we have $i^2 + j^2 + \left(k + \frac{1}{2}\right)^2 = r^2$, which is a contradiction, since $r, i, j, k$ are all integers. □

Lemma 2 helps in characterizing a voxel $p \in S_r^{\mathbb{Z}}$, as stated next.

**Theorem 1.** *$p(i, j, k) \in S_r^{\mathbb{Z}}$ if and only if p is not simple and $i^2 + j^2 + k^2 \in \left[r^2 - \max\{|i|, |j|, |k|\},\ r^2 + \max\{|i|, |j|, |k|\} - 1\right]$.*

*Proof.* Let, w.l.o.g., $p \in \mathbb{Q}_1$. So, $\max\{|i|,|j|,|k|\} = k$. Hence, by Lemma 1 and Lemma 2, $p \in S_r^{\mathbb{Z}_1}$ if and only if $p$ is not simple and

$$-\frac{1}{2} < k - \sqrt{r^2 - (i^2+j^2)} < \frac{1}{2} \tag{3}$$

$$\Leftrightarrow k^2 - k + \frac{1}{4} < r^2 - (i^2+j^2) < k^2 + k + \frac{1}{4}. \tag{4}$$

Since $k^2-k$, $r^2-(i^2+j^2)$, $k^2+k$ are integers, Eq. 4 is true if and only if

$$\begin{aligned} & k^2 - k < r^2 - (i^2+j^2) \leqslant k^2 + k \\ \Leftrightarrow\ & r^2 - k \leqslant i^2 + j^2 + k^2 < r^2 + k, \end{aligned} \tag{5}$$

and hence the proof for 1st q-octant. For other q-octants, the proof is similar. □

Now, to obtain the necessary and sufficient condition of deciding whether a voxel is simple, we need the following theorem.

**Theorem 2.** *A voxel $p(i,j,k)$ with $d_\perp(p, S_r^{\mathbb{R}}) < \frac{1}{2}$ is simple if and only if $i^2 + j^2 + k^2 = r^2 + \max\{|i|,|j|,|k|\} - 1$ and $\mathrm{mid}\{|i|,|j|,|k|\} = \max\{|i|,|j|,|k|\}$, where $\mathrm{mid}\{\cdot\}$ denotes the median element.*

*Proof.* As in the proof of Theorem 1, let, w.l.o.g., $p \in \mathbb{Q}_1$; so, $\mathrm{mid}\{|i|,|j|,|k|\} = j$ and $\max\{|i|,|j|,|k|\} = k$. Let also, $d_\perp(p, S_r^{\mathbb{R}_1}) < \frac{1}{2}$, which implies $p$ satisfies Eq. 5 by Lemma 1 and Lemma 2.

Now, we prove that $p(i,j,k)$ lies on $S_r^{\mathbb{Z}_1}$ and cannot be a simple voxel if $j < k$. For this, first observe that $(i,j,k-1)$ and $(i,j,k+1)$ lie in $\mathbb{Q}_1$, as $j \leqslant k-1$. Next, observe that for any $(i',j') \in \mathbb{Z}^2$, there can be at most one integer value of $k'$ so that $(i',j',k')$ satisfies Eq. 3. This implies that $(i,j,k-1)$ lies in the interior and $(i,j,k+1)$ in the exterior of $S_r^{\mathbb{Z}}$. Hence, discarding $p$ would violate the 2-separableness of $S_r^{\mathbb{Z}}$.

Now, the conditions $i^2+j^2+k^2 = r^2+\max\{|i|,|j|,|k|\}-1$ and $\mathrm{mid}\{|i|,|j|,|k|\} = \max\{|i|,|j|,|k|\}$ imply $(i^2+k^2+k^2) = (r^2+k-1)$, which is true if and only if

$$\begin{aligned} & (i^2 + (k-1)^2 + k^2) = (r^2 - k) \\ \Leftrightarrow\ & (i, k-1, k) \in S_r^{\mathbb{Z}} \text{ by Theorem 1, and } (i,k,k-1) \in S_r^{\mathbb{Z}} \\ \Leftrightarrow\ & (i,k,k) \text{ is simple.} \end{aligned}$$

For $p$ lying in some other octant, the proof follows a similar way. □

Using Theorem 1 and Theorem 2, we get a mathematically refined definition of digital sphere, as stated in the following theorem.

**Theorem 3.** *The voxel set of the digital sphere $S_r^{\mathbb{Z}}$ is given by*

$$\left\{ (i,j,k) \in \mathbb{Z}^3 : r^2 - \max\{|i|,|j|,|k|\} \leqslant i^2+j^2+k^2 < r^2 + \max\{|i|,|j|,|k|\} \right. \\ \left. \wedge \begin{pmatrix} (i^2+j^2+k^2 \neq r^2 + \max\{|i|,|j|,|k|\} - 1) \\ \vee\, (\mathrm{mid}\{|i|,|j|,|k|\} \neq \max\{|i|,|j|,|k|\}) \end{pmatrix} \right\}.$$

## 3 Discrete Spherical Geodesic Path and Circle

Theorem 3 is used to decide in constant time whether a voxel $p(i,j,k)$ belongs to $S_r^{\mathbb{Z}}$. For generating the discrete spherical geodesic path $\boldsymbol{\pi}_r^{\mathbb{Z}}(s,t)$ from a voxel $s \in S_r^{\mathbb{Z}}$ to a voxel $t \in S_r^{\mathbb{Z}}$, we consider the real plane $\Pi_r^{\mathbb{R}}(s,t)$ that passes through $s$, $t$, and the center of $S_r^{\mathbb{Z}}$. Considering voxels as 3-cells, let $I_r^{\mathbb{Z}}(s,t)$ be the set of voxels of $S_r^{\mathbb{Z}}$ intersected by $\Pi_r^{\mathbb{R}}(s,t)$. We have the following lemma for $I_r^{\mathbb{Z}}(s,t)$.

**Lemma 3.** $d_\perp(p, \Pi_r^{\mathbb{R}}(s,t)) \leqslant \frac{3}{2} \ \forall \ p \in I_r^{\mathbb{Z}}(s,t)$.

*Proof.* Let $\delta_e := d_e(p, \Pi_r^{\mathbb{R}}(s,t))$ be the real (Euclidean) distance of the point $p$ from $\Pi_r^{\mathbb{R}}(s,t)$. If $\Pi_r^{\mathbb{R}}(s,t)$ intersects the voxel $p$, then $\delta_e \leqslant \frac{\sqrt{3}}{2}$.

Now, let $\delta_x = d_x(p, \Pi_r^{\mathbb{R}}(s,t)), \delta_y = d_y(p, \Pi_r^{\mathbb{R}}(s,t)), \delta_z = d_z(p, \Pi_r^{\mathbb{R}}(s,t))$. Observe that $\delta_x = \frac{\delta_e}{\cos\theta_x}, \delta_y = \frac{\delta_e}{\cos\theta_y}, \delta_z = \frac{\delta_e}{\cos\theta_z}$, where, $\cos^2\theta_x + \cos^2\theta_y + \cos^2\theta_z = 1$. Here, $\cos\theta_x$ is the angle between the $x$-axis-parallel line through $p$ and the perpendicular on $\Pi_r^{\mathbb{R}}(s,t)$ dropped from $p$, etc. So, the supremum of $d_\perp(p, \Pi_r^{\mathbb{R}}(s,t)) := \min\{\delta_x, \delta_y, \delta_z\}$ corresponds to the infimum of the largest element in $C_\theta := \{\cos\theta_x, \cos\theta_y, \cos\theta_z\}$, and hence to the infimum of the largest element in $C_\theta^{(2)} := \{\cos^2\theta_x, \cos^2\theta_y, \cos^2\theta_z\}$, subject to $\cos^2\theta_x + \cos^2\theta_y + \cos^2\theta_z = 1$. Clearly, the largest element in $C_\theta^{(2)}$ is at least $\frac{1}{3}$, or, the largest element in $C_\theta$ is at least $\frac{1}{\sqrt{3}}$, whence $d_\perp(p, \Pi_r^{\mathbb{R}}(s,t)) \leqslant \delta_e / \frac{1}{\sqrt{3}} = \frac{3}{2}$. □

**Theorem 4.** *For any two voxels $s \in S_r^{\mathbb{Z}}$ and $t \in S_r^{\mathbb{Z}}$, there always exist two 1-connected paths, $\pi_r^{\mathbb{Z}}(s,t)' \subset I_r^{\mathbb{Z}}(s,t)$ and $\pi_r^{\mathbb{Z}}(t,s)'' \subset I_r^{\mathbb{Z}}(s,t)$, such that $\pi_r^{\mathbb{Z}}(s,t)' \cup \pi_r^{\mathbb{Z}}(t,s)''$ forms a 1-connected simple cycle in $I_r^{\mathbb{Z}}(s,t)$.*

*Proof.* Given a continuous surface $A$, there is a unique *supercover* of $A$, defined as the set of all voxels intersecting $A$ [6]. Hence, if $\Pi_r^{\mathbb{Z}}(s,t)$ denotes the *supercover* of $\Pi_r^{\mathbb{R}}(s,t)$, then all the voxels—conceived as 3-cells—that are intersected by $\Pi_r^{\mathbb{R}}(s,t)$, comprise the set $\Pi_r^{\mathbb{Z}}(s,t)$. As shown in [2], the supercover of a plane is 2-separable.

We define $\mathcal{S}_{r^-}^{\mathbb{Z}}$ and $\mathcal{S}_{r^+}^{\mathbb{Z}}$ as the respective interior and exterior of $S_r^{\mathbb{Z}}$. So, by Definition 2, the sets $\mathcal{S}_{r^-}^{\mathbb{Z}}$ and $\mathcal{S}_{r^+}^{\mathbb{Z}}$ are disconnected in 2-neighborhood. Also, let $\Pi_{r^-}^{\mathbb{Z}}(s,t) = \Pi_r^{\mathbb{Z}}(s,t) \cap \mathcal{S}_{r^-}^{\mathbb{Z}}$ and $\Pi_{r^+}^{\mathbb{Z}}(s,t) = \Pi_r^{\mathbb{Z}}(s,t) \cap \mathcal{S}_{r^+}^{\mathbb{Z}}$. Note that $\Pi_{r^-}^{\mathbb{Z}}(s,t)$ is a non-empty set and always contains $o$ for $r \geqslant 1$, since $\Pi_r^{\mathbb{R}}(s,t)$ passes through $o$. This yields

$$\Pi_r^{\mathbb{Z}}(s,t) = \Pi_{r^-}^{\mathbb{Z}}(s,t) \cup I_r^{\mathbb{Z}}(s,t) \cup \Pi_{r^+}^{\mathbb{Z}}(s,t) \tag{6}$$

where, $\Pi_{r^-}^{\mathbb{Z}}(s,t)$, $I_r^{\mathbb{Z}}(s,t)$, and $\Pi_{r^+}^{\mathbb{Z}}(s,t)$ are pairwise disjoint.

Now, as $\mathcal{S}_{r^-}^{\mathbb{Z}}$ and $\mathcal{S}_{r^+}^{\mathbb{Z}}$ are not 2-connected, their respective subsets $\Pi_{r^-}^{\mathbb{Z}}(s,t)$ and $\Pi_{r^+}^{\mathbb{Z}}(s,t)$ are also not 2-connected. So, by Eq. 6, the set $I_r^{\mathbb{Z}}(s,t)$ forms a 2-separating set between $\Pi_{r^-}^{\mathbb{Z}}(s,t)$ and $\Pi_{r^+}^{\mathbb{Z}}(s,t)$, or, equivalently, $I_r^{\mathbb{Z}}(s,t)$ is a 1-connected set that also 2-separates $S_r^{\mathbb{Z}}$. Therefore, there always exists a 1-connected simple path $\pi_r^{\mathbb{Z}}(s,t)' \in I_r^{\mathbb{Z}}(s,t)$ from $s$ to $t$, and another 1-connected simple path $\pi_r^{\mathbb{Z}}(t,s)'' \in I_r^{\mathbb{Z}}(s,t)$ from $t$ to $s$, where $\pi_r^{\mathbb{Z}}(s,t)' \cap \pi_r^{\mathbb{Z}}(t,s)'' = \{s,t\}$. Hence, there always exists a 1-connected simple cycle $(\pi_r^{\mathbb{Z}}(s,t)' \cup \pi_r^{\mathbb{Z}}(t,s)'')$ in $I_r^{\mathbb{Z}}(s,t)$ containing any two voxels $s \in S_r^{\mathbb{Z}}$ and $t \in S_r^{\mathbb{Z}}$. □

From Theorem 4, it is clear that for two given voxels $s \in S_r^{\mathbb{Z}}$ and $t \in S_r^{\mathbb{Z}}$, we get at least two 1-connected paths, $\pi_r^{\mathbb{Z}}(s,t)'$ and $\pi_r^{\mathbb{Z}}(s,t)''$, in $I_r^{\mathbb{Z}}(s,t)$, having no voxels in common, excepting $s$ and $t$. The discrete 3D (integer) circle passing through two given voxels $s$ and $t$ is, therefore, given by $C_r^{\mathbb{Z}}(s,t) = \pi_r^{\mathbb{Z}}(s,t)' \cup \pi_r^{\mathbb{Z}}(t,s)''$. Note that specifying only $s \in S_r^{\mathbb{Z}}$ and $t \in S_r^{\mathbb{Z}}$ would suffice to get $\boldsymbol{\pi}_r^{\mathbb{Z}}(s,t)$, and hence $C_r^{\mathbb{Z}}(s,t)$, since a unique value of $r$ would satisfy Theorem 1 for each of $s$ and $t$.

## 4 Algorithm DSGP

We define *inter-octant distance* $d_{i,j}^{(8)}$ corresponding to $\mathbb{C}_i$ and $\mathbb{C}_j$. With $s \in \mathbb{C}_i$ and $t \in \mathbb{C}_j$, it is given by the count of q-octants crossed by $\boldsymbol{\pi}_r^{\mathbb{Z}}(s,t)$ before entering $\mathbb{C}_j$. Mathematically,

$$d_{i,j}^{(8)} = 1 + \sum_{u=1}^{3} 2^{u-1} \left( c_i^{(u)} \oplus c_j^{(u)} \right) \tag{7}$$

where, $c_i^{(u)} \oplus c_j^{(u)} = 1$ if $c_i^{(u)} \neq c_j^{(u)}$, and 0 otherwise. If $i = j$, then $d_{i,j}^{(8)} = 0$; otherwise, the value of $d_{i,j}^{(8)}$ lies in the interval $[1, 7]$. The maximum value $d_{i,j}^{(8)} = 7$ is obtained when $\mathbb{C}_i$ and $\mathbb{C}_j$ are *diametrically opposite*, i.e., $c_i^{(u)} \neq c_j^{(u)}$ for $u = 1, 2, 3$. The pair $(s,t)$ becomes *antipodal* if their c-octants are diametrically opposite and $s, o, t$ are collinear. Then $\Pi_r^{\mathbb{R}}(s,t)$ has no fixed orientation, and so a third point $q$ on $S_r^{\mathbb{Z}}$ needs to be specified, which would lie in $\boldsymbol{\pi}_r^{\mathbb{Z}}(s,t)$.

Similarly, we define the *intra-octant distance* $d_{i,j}^{(6)}$ between two q-octants, $\mathbb{Q}_i$ and $\mathbb{Q}_j$, when they lie in same c-octant. It provides the count of q-octants containing the geodesic path from any point $s \in \mathbb{Q}_i$ to any point $t \in \mathbb{Q}_j$. According to our representation, it is given by one plus the minimum number of swaps among the elements in $Q_i$, so that, after swaps, the transformed 3-tuple is identical with $Q_j$. Two elements are swapped in $Q_i$ or in any of its intermediate configurations only if the elements are consecutive in $Q_i$ or in that configuration (i.e., 3-tuple). Using $d_{i,j}^{(8)}$ and $d_{i,j}^{(6)}$, we compute the *q-octant distance* $d_{i,j}^{(48)}$ between $s$ and $t$. It gives the count of q-octants containing the geodesic path from $s$ to $t$, irrespective of their positions on the sphere. Its measure turns out to be

$$d_{i,j}^{(48)} = d_{i,j}^{(8)} + d_{i,j}^{(6)} - 1. \tag{8}$$

Combining the above, we simplify the rule of determining the sequence of q-octants containing $\boldsymbol{\pi}_r^{\mathbb{Z}}(s,t)$ as follows. Let $\mathbb{Q}_i$ and $\mathbb{Q}_j$ be the q-octants containing $s$ and $t$, respectively. Then the sequence of q-octants through which $\boldsymbol{\pi}_r^{\mathbb{Z}}(s,t)$ passes, is given by a/the minimum-length sequence of transformations applied on $Q_i$ to attain the configuration $Q_j$. Following are the rules of transformation.

$T_1$. Change the sign of the first element $q_i^{(1)}$ in $Q_i$ (or its intermediate configuration) only if $\sigma[q_i^{(1)}] \neq \sigma[q_j^{(1)}]$. This signifies transition from one half-space (or, c-octant) to another half-space.

$T_2$. Swap two elements in $Q_i$ (or its intermediate configuration) only if they are consecutive. This signifies transition from one q-octant to its adjacent q-octant.

From the sequence of q-octants obtained by the required transformations, we determine the q-octant $\mathbb{Q}_{i'}$ immediately next to the q-octant $\mathbb{Q}_i$ of $s$. We use the 3-tuples corresponding to $\mathbb{Q}_i$ and $\mathbb{Q}_{i'}$ for computing the direction vector $\mathbf{d}_s := (d_s^{(1)}, d_s^{(2)}, d_s^{(3)}) \in \{+\mathtt{1}, -\mathtt{1}, \pm\mathtt{1}\}^3$. It is required to find the candidate voxels that are 1-adjacent to $s$ ($\mathbb{A}_1(s)$), belong to $I_r^{\mathbb{Z}}(s,t)$, and is directed towards the shorter between the two possible geodesics from $s$ to $t$ (Theorem 4). The elements $d_s^{(1)}, d_s^{(2)}, d_s^{(3)}$ correspond to the moves along $x$-, $y$-, $z$-axes, respectively. The notation $+\mathtt{1}$ signifies that there can be a unit move or no move (from $s$) along the positive axis of the corresponding coordinate; similarly, $-\mathtt{1}$ signifies a unit move or no move along the negative axis, and $\pm\mathtt{1}$ signifies no move or a unit move along positive or negative axis. In case of more than one minimum-length sequence of q-octants from $\mathbb{Q}_i$ to $\mathbb{Q}_j$, we consider the q-octant nearest to $\mathbb{Q}_i$ and common to these sequences, for computing $\mathbf{d}_s$. The rationale is that only one of these sequences would be intersected by $\mathit{\Pi}_r^{\mathbb{R}}(s,t)$, and hence the q-octant common to these sequences is used. The following examples clarify the idea.

*Example 2.* See Fig. 2. Given $s(10,-2,6) \in \mathbb{Q}_{15}$ and $t(-3,10,6) \in \mathbb{Q}_{12}$, their respective 3-tuples are $Q_{15} := (-\mathtt{y}, +\mathtt{z}, +\mathtt{x})$ and $Q_{12} := (-\mathtt{x}, +\mathtt{z}, +\mathtt{y})$. The minimum-length sequence of transformations corresponding to $\boldsymbol{\pi}_r^{\mathbb{Z}}(s,t)$ is:
$(-\mathtt{y}, +\mathtt{z}, +\mathtt{x}) \xrightarrow{T_1} (+\mathtt{y}, +\mathtt{z}, +\mathtt{x}) \xrightarrow{T_2} (+\mathtt{y}, +\mathtt{x}, +\mathtt{z}) \xrightarrow{T_2} (+\mathtt{x}, +\mathtt{y}, +\mathtt{z}) \xrightarrow{T_2} (+\mathtt{x}, +\mathtt{z}, +\mathtt{y}) \xrightarrow{T_1} (-\mathtt{x}, +\mathtt{z}, +\mathtt{y})$, or, $Q_{15} \xrightarrow{T_1} Q_3 \xrightarrow{T_2} Q_2 \xrightarrow{T_2} Q_1 \xrightarrow{T_2} Q_6 \xrightarrow{T_1} Q_{12}$.
Notice that there is another minimum-length sequence: $(-\mathtt{y}, +\mathtt{z}, +\mathtt{x}) \xrightarrow{T_1} (+\mathtt{y}, +\mathtt{z}, +\mathtt{x}) \xrightarrow{T_2} (+\mathtt{z}, +\mathtt{y}, +\mathtt{x}) \xrightarrow{T_2} (+\mathtt{z}, +\mathtt{x}, +\mathtt{y}) \xrightarrow{T_2} (+\mathtt{x}, +\mathtt{z}, +\mathtt{y}) \xrightarrow{T_2} (-\mathtt{x}, +\mathtt{z}, +\mathtt{y})$, which implies $Q_{15} \xrightarrow{T_1} Q_3 \xrightarrow{T_2} Q_4 \xrightarrow{T_2} Q_5 \xrightarrow{T_2} Q_6 \xrightarrow{T_2} Q_{12}$.
Either of these implies that the q-octant next to $\mathbb{Q}_{15}$ through which $\boldsymbol{\pi}_r^{\mathbb{Z}}(s,t)$ passes, is $\mathbb{Q}_3$. Since $Q_{15} = (-\mathtt{y}, +\mathtt{z}, +\mathtt{x})$ and $Q_3 = (+\mathtt{y}, +\mathtt{z}, +\mathtt{x})$, the $y$-coordinate of each voxel $p \in \mathbb{A}_1(s) \cap I_r^{\mathbb{Z}}(s,t)$, cannot ever decrease. On the contrary, the $x$- and the $z$-coordinates of $p$ have no such restriction. Hence, the direction vector $\mathbf{d}_s$ is chosen as $(\pm\mathtt{1}, +\mathtt{1}, \pm\mathtt{1})$.
*Example 3.* Let $s \in \mathbb{Q}_1$ and $t \in \mathbb{Q}_4$. So, $Q_1 = (+\mathtt{x}, +\mathtt{y}, +\mathtt{z})$ and $Q_4 = (+\mathtt{z}, +\mathtt{y}, +\mathtt{x})$. We have two minimum-length sequence of transformations: (i) $Q_1 \xrightarrow{T_2} Q_2 \xrightarrow{T_2} Q_3 \xrightarrow{T_2} Q_4$; (ii) $Q_1 \xrightarrow{T_2} Q_6 \xrightarrow{T_2} Q_5 \xrightarrow{T_2} Q_4$.
Contrary to Example 2, here the q-octants following $\mathbb{Q}_1$ in two cases are different: $\mathbb{Q}_2$ for (i) and $\mathbb{Q}_6$ for (ii). So, we look ahead until there is a matching q-octant, i.e., $\mathbb{Q}_4$ in this case. We compute $\mathbf{d}_s$ as the relative shifts in positions of the coordinate values in $Q_4$. In $Q_1$, the 1st element is $+\mathtt{x}$, which is shifted to 3rd position in $Q_4$. So, the 1st element in $\mathbf{d}_s$ becomes $+\mathtt{1}$, and by similar reasoning with the 2nd and the 3rd elements, we get $\mathbf{d}_s = (+\mathtt{1}, \pm\mathtt{1}, -\mathtt{1})$.

**Analysis.** See Algorithm 1 and its demonstration in Fig. 2. The adjacency list $L$ of the underlying undirected graph $G(V,E)$ is prepared based on 1-adjacency of the voxels in $I_r^{\mathbb{Z}}(s,t)$. The vertices adjacent to each $u \in V$ are inserted in the

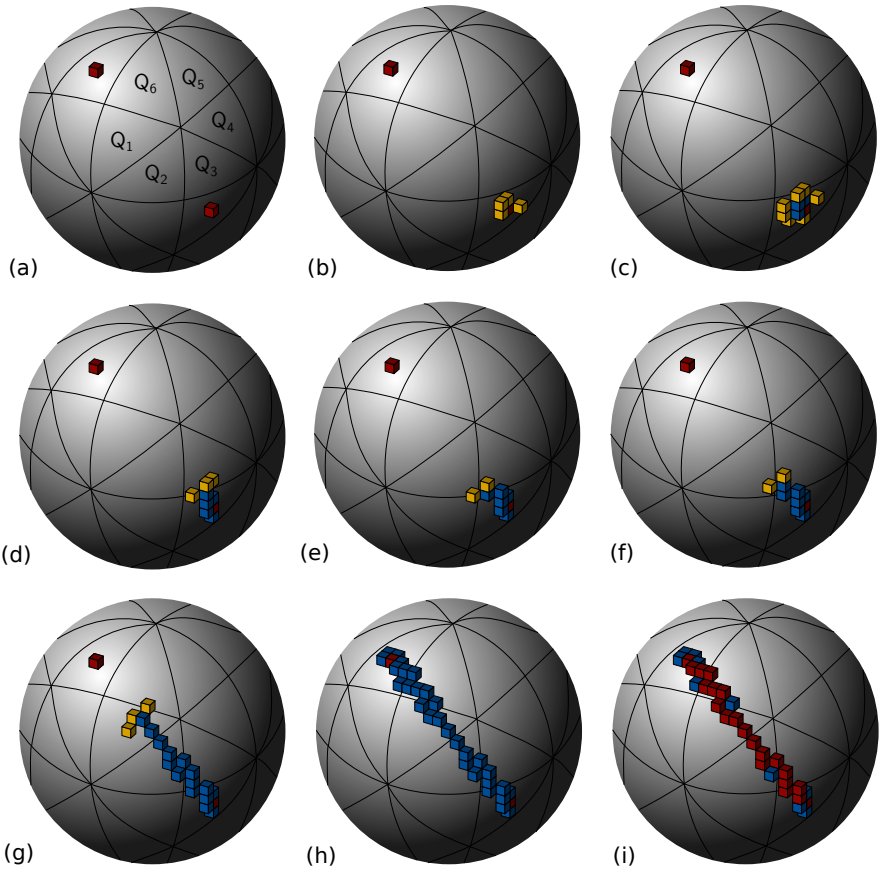


**Fig. 2.** A demonstration of the proposed algorithm for $r = 12$. (a) $s(10, -2, 6) \in \mathbb{Q}_{15}$, $t(-3, 10, 6) \in \mathbb{Q}_{12}$. (b) Yellow: $S_r^{\mathbb{Z}} \cap \mathbb{A}_1(s)$. (c) Blue: $S_r^{\mathbb{Z}} \cap \mathbb{A}_1(s) \cap I_r^{\mathbb{Z}}(s,t)$, Yellow: $\{p \in \mathbb{A}_1(q) : q \text{ is Blue}\}$. (d-h) Blue: Progress of Procedure MakeAdjList for $I_r^{\mathbb{Z}}(s,t)$. (i) Red: $\boldsymbol{\pi}_r^{\mathbb{Z}}(s,t) \subset I_r^{\mathbb{Z}}(s,t)$.

adjacency chain $L[u]$ of $u$ in non-increasing order of their isothetic distances from $\mathit{\Pi}_r^{\mathbb{R}}(s,t)$, (MakeAdjList, Line 9). This is needed to maintain locally minimum isothetic distance from $\mathit{\Pi}_r^{\mathbb{R}}(s,t)$ while running Prioritized-BFS (Algorithm 1, Line 3). In Line 8 of MakeAdjList, Theorem 1 is used to determine the voxels that are 1-adjacent with the current voxel and belong to $S_r^{\mathbb{Z}}$, in constant time. Thus, MakeAdjList and Prioritized-BFS consumes $O(n)$ time each, where $n$ is the number of voxels comprising $\boldsymbol{\pi}_r^{\mathbb{Z}}(s,t)$. The direction vector $\mathbf{d}_s$ is computed from the sequence(s) in no more than $O(n)$ time complexity. Hence, the total time complexity of Algorithm DSGP is linear in the length of $\boldsymbol{\pi}_r^{\mathbb{Z}}(s,t)$.

## 5 Results

The proposed algorithm is implemented in C in Ubuntu 12.04 32-bit, Kernel Linux 3.2.0-31-generic-pae, GNOME 3.4.2, Intel® Core™ i5-2400 CPU 3.10GHz.

**Algorithm 1:** DSGP (Discrete Spherical Geodesic Path).

**Input**: voxel $s \in S_r^{\mathbb{Z}}$, voxel $t \in S_r^{\mathbb{Z}}$, such that $(s,t)$ is not an antipodal pair
**Output**: $\boldsymbol{\pi}_r^{\mathbb{Z}}(s,t)$ as a voxel sequence

```
1  d_s ← FindDirection(s, t)
2  L ← MakeAdjList(s, t, d_s)
3  π_r^ℤ(s, t) ← Prioritized-BFS(s, t, L)
```

**Procedure** FindDirection(voxel $s$, voxel $t$)

**Output**: Direction vector $\mathbf{d}_s$

```
1  Q_i ← FindQoct(s), Q_j ← FindQoct(t)
2  S_{i,j} ← minimum-length q-octant sequence from Q_i to Q_j
3  if S_{i,j} is unique then
4      Q_{i'} ← 2nd element (q-octant) in S_{i,j}
5  else
6      Q_{i'} ← common element in the sequences {S_{i,j}} nearest to Q_i
7  Compute d_s from positions of the corresponding elements in Q_i and Q_{i'}
8  return d_s
```

**Procedure** MakeAdjList(voxel $s$, voxel $t$, $\mathbf{d}_s$)

**Output**: Adjacency list $L$ of $I_r^{\mathbb{Z}}(s,t)$

```
1  visited[s] ← TRUE
2  Q ← {q : (q ∈ S_r^ℤ) ∧ (q ∈ Π_r^ℤ(s,t)) ∧ ((s,q) conforms d_s)}
3  for each q ∈ Q do
4      visited[q] ← FALSE
5  while Q ≠ ∅ do
6      voxel p ← Dequeue(Q), visited[p] ← TRUE
7      for each voxel q in 1-neighborhood of p do
8          if (q ∈ S_r^ℤ) ∧ (q ∈ Π_r^ℤ(s,t)) then
9              insert q in L[p] in non-increasing order of d_⊥(q, Π_r^ℝ(s,t))
10         if visited[q] = FALSE then
11             Enqueue(Q, q)
12 return L
```

As the algorithm is of linear time complexity and readily implementable with primitive operations in the integer space, it computes the spherical geodesic paths and 3D circles in $\mathbb{Z}^3$ quite fast and efficiently. To demonstrate this, a summary of some experimental results is given in Appendix. For radius $r$ ranging from 10 to 1000, different source and destination points are chosen, and their geodesic paths are computed. For each path $\boldsymbol{\pi}_r^{\mathbb{Z}}(s,t)$, its length $|\boldsymbol{\pi}_r^{\mathbb{Z}}(s,t)|$, measured in terms of number of voxels comprising the path, is shown, along with the corresponding q-octant distance, $d_{i,j}^{(48)}$. The CPU time, measured in milliseconds, reflects the linear-time behavior of the algorithm, as explained in Section 4.

The figure in Appendix shows a set of discrete spherical geodesics and their corresponding circles produced by the algorithm. Note that a discrete geodesic

circle can be obtained by taking the union of the path $\boldsymbol{\pi}_r^{\mathbb{Z}}(s,t)$ with its complementary path, i.e., $\boldsymbol{\pi}_r^{\mathbb{Z}}(t,s)$, taken in the same order of cyclic movement. Clearly, such a circle would always include $s$ and $t$. However, the inclusion of $t$ is not ensured if we ignore $t$ during Prioritized-BFS and moves forward until the traversal returns to $s$, although the resultant geodesic circle would comprise voxels lying within an isothetic distance of $\frac{3}{2}$ from $\Pi_r^{\mathbb{R}}(s,t)$.

## 6 Conclusion

We have shown how number-theoretic characterization helps in developing efficient algorithms related to discrete geodesics on a spherical surface. The problems of finding *iso-contours* and of *geodesic distance query*, defined and attempted in 3D real space [17, 18], are also pertinent in 3D digital space. The technique introduced in this paper may be extended to solve such problems with efficiency and theoretical guarantee.

## References

[1] Balasubramanian, M., Polimeni, J.R., Schwartz, E.L.: Exact geodesics and shortest paths on polyhedral surfaces. IEEE TPAMI 31, 1006–1016 (2009)
[2] Brimkov, V., Coeurjolly, D., Klette, R.: Digital planarity—A review. Discrete Appl. Math. 155, 468–495 (2007)
[3] Bülow, T., Klette, R.: Digital curves in 3D space and a linear-time length estimation algorithm. IEEE TPAMI 24, 962–970 (2002)
[4] Chen, J., Han, Y.: Shortest paths on a polyhedron. In: Proc. SoCG, pp. 360–369 (1990)
[5] Coeurjolly, D., Miguet, S., Tougne, L.: 2D and 3D visibility in discrete geometry: An application to discrete geodesic paths. PRL 25, 561–570 (2004)
[6] Cohen-Or, D., Kaufman, A.: Fundamentals of surface voxelization. GMIP 57, 453–461 (1995)
[7] Coxeter, H.S.M.: Regular Polytopes. Dover Pub. (1973)
[8] Kimmel, R., Sethian, J.A.: Computing geodesic paths on manifolds. Proc. Natl. Acad. Sci. USA, 8431–8435 (1998)
[9] Klette, R., Rosenfeld, A.: Digital Geometry: Geometric Methods for Digital Picture Analysis. Morgan Kaufmann, San Francisco (2004)
[10] Li, F., Klette, R.: Analysis of the rubberband algorithm. Image Vision Comput. 25, 1588–1598 (2007)
[11] Martínez, D., Velho, L., Carvalho, P.C.: Computing geodesics on triangular meshes. Computers & Graphics 29, 667–675 (2005)
[12] Mitchell, J.S.B., Mount, D.M., Papadimitriou, C.H.: The discrete geodesic problem. SIAM J. Comput. 16, 647–668 (1987)
[13] Polthier, K., Schmies, M.: Straightest geodesics on polyhedral surfaces. In: ACM SIGGRAPH 2006 Courses, pp. 30–38 (2006)
[14] Surazhsky, V., Surazhsky, T., Kirsanov, D., Gortler, S.J., Hoppe, H.: Fast exact and approximate geodesics on meshes. ACM TOG 24, 553–560 (2005)
[15] Toutant, J.L., Andres, E., Roussillon, T.: Digital circles, spheres and hyperspheres: From morphological models to analytical characterizations and topological properties. Discrete Appl. Math. 161, 2662–2677 (2013)
[16] Xin, S.Q., Wang, G.J.: Improving Chen and Han's algorithm on the discrete geodesic problem. ACM TOG 28, Art. 104 (2009)

[17] Xin, S.Q., Ying, X., He, Y.: Constant-time all-pairs geodesic distance query on triangle meshes. In: Proc. I3D 2012, pp. 31–38 (2012)
[18] Ying, X., Wang, X., He, Y.: Saddle vertex graph (SVG): A novel solution to the discrete geodesic problem. ACM TOG 32, Art. 170 (2013)
[19] Ying, X., Xin, S.Q., He, Y.: Parallel Chen-Han (PCH) algorithm for discrete geodesics. ACM TOG 33, Art. 9 (2014)

## Appendix

**Table.** C-octants and Q-octants

| C-oct | Q-octants | Notation |
|---|---|---|
| $\mathbb{C}_1$ | $\mathbb{Q}_1, \ldots, \mathbb{Q}_6$ | $+++$ |
| $\mathbb{C}_2$ | $\mathbb{Q}_7, \ldots, \mathbb{Q}_{12}$ | $-++$ |
| $\mathbb{C}_3$ | $\mathbb{Q}_{13}, \ldots, \mathbb{Q}_{18}$ | $+-+$ |
| $\mathbb{C}_4$ | $\mathbb{Q}_{19}, \ldots, \mathbb{Q}_{24}$ | $--+$ |
| $\mathbb{C}_5$ | $\mathbb{Q}_{25}, \ldots, \mathbb{Q}_{30}$ | $++-$ |
| $\mathbb{C}_6$ | $\mathbb{Q}_{31}, \ldots, \mathbb{Q}_{36}$ | $-+-$ |
| $\mathbb{C}_7$ | $\mathbb{Q}_{37}, \ldots, \mathbb{Q}_{42}$ | $+--$ |
| $\mathbb{C}_8$ | $\mathbb{Q}_{43}, \ldots, \mathbb{Q}_{48}$ | $---$ |

| Q-oct | Notation | Q-oct | Notation | Q-oct | Notation |
|---|---|---|---|---|---|
| $\mathbb{Q}_1$ | $(+x,+y,+z)$ | $\mathbb{Q}_2$ | $(+y,+x,+z)$ | $\mathbb{Q}_3$ | $(+y,+z,+x)$ |
| $\mathbb{Q}_7$ | $(-x,+y,+z)$ | $\mathbb{Q}_8$ | $(+y,-x,+z)$ | $\mathbb{Q}_9$ | $(+y,+z,-x)$ |
| $\mathbb{Q}_{13}$ | $(+x,-y,+z)$ | $\mathbb{Q}_{14}$ | $(-y,+x,+z)$ | $\mathbb{Q}_{15}$ | $(-y,+z,+x)$ |
| $\mathbb{Q}_{19}$ | $(-x,-y,+z)$ | $\mathbb{Q}_{20}$ | $(-y,-x,+z)$ | $\mathbb{Q}_{21}$ | $(-y,+z,-x)$ |
| $\mathbb{Q}_{25}$ | $(+x,+y,-z)$ | $\mathbb{Q}_{26}$ | $(+y,+x,-z)$ | $\mathbb{Q}_{27}$ | $(+y,-z,+x)$ |
| $\mathbb{Q}_{31}$ | $(-x,+y,-z)$ | $\mathbb{Q}_{32}$ | $(+y,-x,-z)$ | $\mathbb{Q}_{33}$ | $(+y,-z,-x)$ |
| $\mathbb{Q}_{37}$ | $(+x,-y,-z)$ | $\mathbb{Q}_{38}$ | $(-y,+x,-z)$ | $\mathbb{Q}_{39}$ | $(-y,-z,+x)$ |
| $\mathbb{Q}_{43}$ | $(-x,-y,-z)$ | $\mathbb{Q}_{44}$ | $(-y,-x,-z)$ | $\mathbb{Q}_{45}$ | $(-y,-z,-x)$ |

| Q-oct | Notation | Q-oct | Notation | Q-oct | Notation |
|---|---|---|---|---|---|
| $\mathbb{Q}_4$ | $(+z,+y,+x)$ | $\mathbb{Q}_5$ | $(+z,+x,+y)$ | $\mathbb{Q}_6$ | $(+x,+z,+y)$ |
| $\mathbb{Q}_{10}$ | $(+z,+y,-x)$ | $\mathbb{Q}_{11}$ | $(+z,-x,+y)$ | $\mathbb{Q}_{12}$ | $(-x,+z,+y)$ |
| $\mathbb{Q}_{16}$ | $(+z,-y,+x)$ | $\mathbb{Q}_{17}$ | $(+z,+x,-y)$ | $\mathbb{Q}_{18}$ | $(+x,+z,-y)$ |
| $\mathbb{Q}_{22}$ | $(+z,-y,-x)$ | $\mathbb{Q}_{23}$ | $(+z,-x,-y)$ | $\mathbb{Q}_{24}$ | $(-x,+z,-y)$ |
| $\mathbb{Q}_{28}$ | $(-z,+y,+x)$ | $\mathbb{Q}_{29}$ | $(-z,+x,+y)$ | $\mathbb{Q}_{30}$ | $(+x,-z,+y)$ |
| $\mathbb{Q}_{34}$ | $(-z,+y,-x)$ | $\mathbb{Q}_{35}$ | $(-z,-x,+y)$ | $\mathbb{Q}_{36}$ | $(-x,-z,+y)$ |
| $\mathbb{Q}_{40}$ | $(-z,-y,+x)$ | $\mathbb{Q}_{41}$ | $(-z,+x,-y)$ | $\mathbb{Q}_{42}$ | $(+x,-z,-y)$ |
| $\mathbb{Q}_{46}$ | $(-z,-y,-x)$ | $\mathbb{Q}_{47}$ | $(-z,-x,-y)$ | $\mathbb{Q}_{48}$ | $(-x,-z,-y)$ |

**Table.** Summary of results

| $r$ | $s$ and its q-octant | | $t$ and its q-octant | | $\lvert\boldsymbol{\pi}_r^{\mathbb{Z}}(s,t)\rvert$ | $d_{i,j}^{(48)}$ | Time ($\mu s$) |
|---|---|---|---|---|---|---|---|
| 10 | $(0,3,10)$ | $\mathbb{Q}_1$ | $(4,6,7)$ | $\mathbb{Q}_1$ | 7 | 0 | 53 |
| 10 | $(4,-4,8)$ | $\mathbb{Q}_{13}$ | $(2,-9,4)$ | $\mathbb{Q}_{18}$ | 8 | 1 | 61 |
| 10 | $(7,1,7)$ | $\mathbb{Q}_2$ | $(-3,7,-6)$ | $\mathbb{Q}_{36}$ | 21 | 6 | 81 |
| 20 | $(1,5,19)$ | $\mathbb{Q}_1$ | $(11,12,12)$ | $\mathbb{Q}_1$ | 16 | 0 | 111 |
| 20 | $(-4,10,17)$ | $\mathbb{Q}_7$ | $(-20,3,2)$ | $\mathbb{Q}_{10}$ | 24 | 3 | 145 |
| 20 | $(-7,3,-18)$ | $\mathbb{Q}_{32}$ | $(4,-10,17)$ | $\mathbb{Q}_{13}$ | 52 | 8 | 330 |
| 50 | $(0,-12,49)$ | $\mathbb{Q}_{13}$ | $(8,-18,46)$ | $\mathbb{Q}_{13}$ | 11 | 0 | 84 |
| 50 | $(30,1,40)$ | $\mathbb{Q}_2$ | $(46,18,8)$ | $\mathbb{Q}_4$ | 40 | 2 | 261 |
| 50 | $(35,-35,-4)$ | $\mathbb{Q}_{41}$ | $(-12,-13,47)$ | $\mathbb{Q}_{19}$ | 81 | 4 | 445 |
| 100 | $(24,61,-76)$ | $\mathbb{Q}_{25}$ | $(57,58,-58)$ | $\mathbb{Q}_{25}$ | 34 | 0 | 167 |
| 100 | $(-39,-48,-79)$ | $\mathbb{Q}_{43}$ | $(-88,-17,-45)$ | $\mathbb{Q}_{45}$ | 66 | 2 | 315 |
| 100 | $(-11,78,61)$ | $\mathbb{Q}_{12}$ | $(98,-17,7)$ | $\mathbb{Q}_{16}$ | 170 | 6 | 1000 |
| 200 | $(116,115,115)$ | $\mathbb{Q}_3$ | $(176,62,73)$ | $\mathbb{Q}_3$ | 93 | 0 | 392 |
| 200 | $(33,33,194)$ | $\mathbb{Q}_1$ | $(199,14,11)$ | $\mathbb{Q}_4$ | 242 | 3 | 1292 |
| 200 | $(46,161,110)$ | $\mathbb{Q}_6$ | $(-87,-2,180)$ | $\mathbb{Q}_{20}$ | 230 | 4 | 1677 |
| 500 | $(-13,406,291)$ | $\mathbb{Q}_{12}$ | $(-250,340,268)$ | $\mathbb{Q}_{12}$ | 239 | 0 | 1178 |
| 500 | $(50,-494,58)$ | $\mathbb{Q}_{18}$ | $(171,-226,412)$ | $\mathbb{Q}_{13}$ | 439 | 1 | 2925 |
| 500 | $(-31,433,248)$ | $\mathbb{Q}_{12}$ | $(117,-171,-455)$ | $\mathbb{Q}_{37}$ | 1142 | 8 | 33347 |
| 1000 | $(25,-929,368)$ | $\mathbb{Q}_{18}$ | $(539,-637,551)$ | $\mathbb{Q}_{18}$ | 628 | 0 | 5159 |
| 1000 | $(384,917,-104)$ | $\mathbb{Q}_{29}$ | $(110,504,-857)$ | $\mathbb{Q}_{25}$ | 892 | 2 | 7771 |
| 1000 | $(932,300,-204)$ | $\mathbb{Q}_{28}$ | $(-637,705,311)$ | $\mathbb{Q}_{11}$ | 1889 | 5 | 61852 |

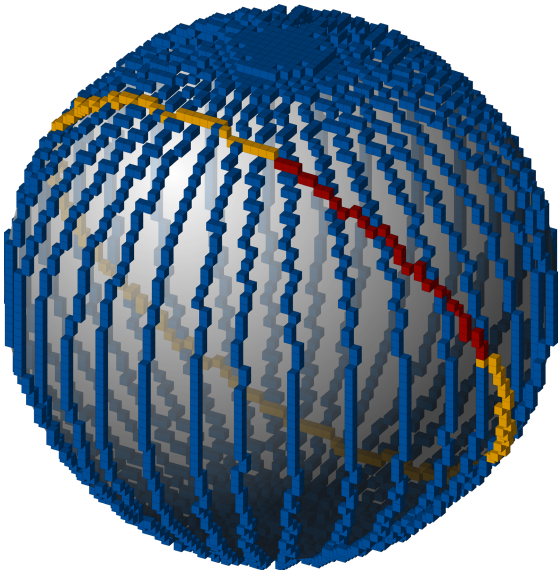

**Figure.** Discrete spherical geodesics and their corresponding circles for $r = 30$. The sequence of red voxels is $\boldsymbol{\pi}_r^{\mathbb{Z}}(s,t)$ with $s(8,25,14) \in \mathbb{Q}_6$ and $t(29,3,6) \in \mathbb{Q}_3$, which, when combined with $\boldsymbol{\pi}_r^{\mathbb{Z}}(t,s)$, shown in yellow, yields the discrete 3D geodesic circle passing through $s$, $t$, and centered at $o$. Shown in blue are 16 longitude circles produced by extending the geodesics from source points taken from the discrete great circle on $zx$-plane to destination point $t(0,30,0)$ for each.